





Article

Synthesis, Mass Spectroscopy Detection, and Density Functional Theory Investigations of the Gd Endohedral Complexes of C₈₂ Fullerenols

Anastasiya A. Shakirova¹, Felix N. Tomilin^{1,2} , Vladimir A. Pomogaev^{3,4}, Natalia G. Vnukova^{1,2}, Grigory N. Churilov^{1,2}, Nadezhda S. Kudryasheva^{1,5} , Olga N. Tchaikovskaya³ , Sergey G. Ovchinnikov^{1,2}  and Pavel V. Avramov^{4,*}

- ¹ Department of Biophysics, School of Engineering Physics and Radio Electronics, School of Petroleum and Gas Engineering, Siberian Federal University, pr. Svobodny 79, 660041 Krasnoyarsk, Russia; anastasiya.shakirova.97@mail.ru (A.A.S.); felixnt@gmail.com (F.N.T.); nata_hd@rambler.ru (N.G.V.); churilov@iph.krasn.ru (G.N.C.); n-qdr@yandex.ru (N.S.K.); sgo@iph.krasn.ru (S.G.O.)
 - ² Krasnoyarsk Scientific Center, Kirensky Institute of Physics, Siberian Branch, Russian Academy of Sciences, Akademgorodok 50, 660036 Krasnoyarsk, Russia
 - ³ Department of Physics, National Research Tomsk State University, Lenina Ave. 36, 634050 Toms, Russia; helper@gmail.com (V.A.P.); tchon@phys.tsu.ru (O.N.T.)
 - ⁴ Department of Chemistry and Green-Nano Materials Research Center, Kyungpook National University, 80 Daehak-ro, Buk-gu, Daegu 41566, Korea
 - ⁵ Krasnoyarsk Scientific Center, Institute of Biophysics, Siberian Branch, Russian Academy of Sciences, Akademgorodok 50/50, 660036 Krasnoyarsk, Russia
- * Correspondence: paul.veniaminovich@knu.ac.kr



Citation: Shakirova, A.A.; Tomilin, F.N.; Pomogaev, V.A.; Vnukova, N.G.; Churilov, G.N.; Kudryasheva, N.S.; Tchaikovskaya, O.N.; Ovchinnikov, S.G.; Avramov, P.V. Synthesis, Mass Spectroscopy Detection, and Density Functional Theory Investigations of the Gd Endohedral Complexes of C₈₂ Fullerenols. *Computation* **2021**, *9*, 58. <https://doi.org/10.3390/computation9050058>

Academic Editor: Karlheinz Schwarz

Received: 16 April 2021

Accepted: 12 May 2021

Published: 17 May 2021

Publisher's Note: MDPI stays neutral with regard to jurisdictional claims in published maps and institutional affiliations.



Copyright: © 2021 by the authors. Licensee MDPI, Basel, Switzerland. This article is an open access article distributed under the terms and conditions of the Creative Commons Attribution (CC BY) license (<https://creativecommons.org/licenses/by/4.0/>).

Abstract: Gd endohedral complexes of C₈₂ fullerenols were synthesized and mass spectrometry analysis of their composition was carried out. It was established that the synthesis yields a series of fullerenols Gd@C₈₂O_x(OH)_y ($x = 0, 3$; $y = 8, 16, 24, 36, 44$). The atomic and electronic structure and properties of the synthesized fullerenols were investigated using the density functional theory calculations. It was shown that the presence of endohedral gadolinium increases the reactivity of fullerenols. It is proposed that the high-spin endohedral fullerenols are promising candidates for application in magnetic resonance imaging.

Keywords: endohedral fullerenes; density functional theory; antioxidant activity; reactive oxygen species; magnetic resonance imaging

1. Introduction

Studies of the properties of fullerenes and fullerene derivatives made it possible to determine the areas of their applications [1–14], including biomedical ones. The main biomedical feature of fullerenes and most of their derivatives is the low toxicity and the ability to be removed from the body [4]. In particular, pristine fullerenes [15] demonstrated low toxicity without substantial health risks for prolonged exposure under good hygiene conditions. It was shown that C₆₀ fullerenols demonstrate some toxicity due to the generation of reactive oxygen species caused by photoexcitation [16]. In particular, it was found that endohedral Gd@C₈₂(OH)₂₂ species exhibited very low toxicity in tumor-bearing mice [17]. It was shown that most of the pristine and functionalized fullerenes are not overtly toxic, unless photoexcited or used at very high concentrations that are unlikely to be encountered environmentally or during therapy. The geometry and electronic structure of fullerenes allow them to form compounds containing various pharmacophore groups, which can easily pass to the excited state under the action of different physical and chemical factors and enclose metal atoms into their carbon cage with the formation of so-called endohedral metallofullerenes. The endohedral metal complexes are characterized by chemical stability, paramagnetism, and large specific surface, which can be easily functionalized [18].

Various functional groups can be attached to a fullerene cage, which makes it possible to obtain water-soluble fullerene derivatives. Fullerenols, due to their hydrophilic properties and ability to bind free radicals, can be used in chemotherapy, treatment of neurodegenerative diseases, and radiology [4,8,9,18]. Theoretical Molecular Dynamics (MD) simulations [19] of $[C_{60}(OH)_n]$, where $n = 2-30$ in aqueous solutions and survey of experimental data [20] demonstrate highly negative solvation free energies which directly indicate the thermodynamic feasibility of fullerenols in water solutions.

In particular, hydroxylated fullerenes (fullerenols) exhibit pronounced antioxidant activity [3]. Fullerenols can react with most of the physiologically significant reactive oxygen species (ROS), including the OH^\bullet , $O_2^{\bullet-}$, and H^\bullet radicals. Fullerenols can simultaneously contain the functional groups that can form radicals in aqueous solutions and anionic groups [4]. The calculation showed that the antioxidant activity with OH^\bullet depends on the distribution of hydroxyls over the C_{60} fullerene cage. The fullerenols, in which the hydroxyl distribution lowers the redox potential ϵ , have the high trapping activity.

A number of functional groups on the fullerene cage (carcass) are critical for the fullerenes biological activity. Eroepkin and co-workers [21] studied the bioeffects of hydroxylated C_{60} fullerene derivatives $C_{60}(OH)_{12-14}$, $C_{60}(OH)_{18-24}$, $C_{60}(OH)_{30-38}$. The authors did not find bioactivity of $C_{60}(OH)_{12-14}$, while fullereneol $C_{60}(OH)_{18-24}$ demonstrated maximal antiviral and protective properties. Kovel et al. [22] revealed a lower toxicity and higher antioxidant activity of fullerenols with fewer oxygen groups (24–28), as compared to fullerenols with the higher number of oxygen groups (40–42). The difference was attributed to the fullerenols catalytic activity via reversible electron acceptance, radical trapping, and balance of ROSs. Involvement of an exohedral atom of Fe to the structure of $C_{60}O_{2-4}(OH)_{20-24}$ increased its toxicity and decreased antioxidant activity [23]. The antioxidant effect of highly diluted fullereneol solutions on bacterial cells was attributed to hormesis phenomenon [24]. It was concerned with stimulation of adaptive response of cells under low-concentration exposures. Sequence analysis of 16S ribosomal RNA was carried out in this study; it did not reveal mutations in bacterial DNA. Additionally, it was shown [25] that the antioxidant ability of natural detoxifying agent, humic substances, was lower and time-dependent, in contrast to fullereneol $C_{60}O_{2-4}(OH)_{20-24}$.

The $Gd@C_{82}$ endohedral fullerene complex and its derivatives are widely used in biomedicine [1–9]. The water-soluble gadolinium-containing metallofullerene derivatives can be excellent candidates to be used as novel magnetic resonance imaging (MRI) contrast agents, since they are characterized by the high relaxing ability and encapsulation of lanthanide ions (Gd^{3+}), which prevents their release into the bioenvironment [5]. The most widely used gadolinium-containing compounds are gadodiamide, gadopentetate dimeglumine, gadoterate meglumine, etc. [26,27]; however, there are fears that these substances may be toxic [27]. The metallofullerene derivatives trap toxic Gd^{3+} ions into an inert yet strong carbon cage preventing their release and exhibit the 10 to 40 times higher proton relaxation ability as compared with that of conventional contrast agents and, in some cases, the much longer retention of the glioma brain tumor in mouse models [28].

Gadolinium endohedral complex $Gd@C_{82}$ increases the magnetic relaxivity of the contrast agent, which is a prerequisite for improved image contrast at lower gadolinium concentrations [29]. It was shown that Gd metallofullereneol in combination with chemotherapy improves the effectiveness of cancer therapy [30]. Gadolinium ions can inhibit calcium channels and exhibit neurological and cardiovascular toxicity [31]. To be used in clinical settings, the gadolinium ion must be placed in a chelating medium, which tightly binds the metal, but allows water to interact with unpaired gadolinium spins. The conventional approach implies the use of polyfunctional ligands, which strongly coordinate the Gd^{3+} ion, but allow at least one water molecule to directly bind to Gd^{3+} [5]. Due to the complexity of the synthesis of fullerenols with the gadolinium guest atom inside a carbon cage, the use of these compounds is still limited. Nevertheless, the $Gd@C_{82}O_x(OH)_y$ fullereneol is a good candidate for biomedical applications, since it has good solubility in water. Gadolinium

enclosed in a carbon cage becomes nontoxic due to the easy removal of fullerenols from the body. In addition, a fullereneol can act as a substance for struggling against the ROSs.

In this work, the density functional theory (DFT) calculations were used to study the equilibrium atomic geometry and electronic structure of Gd endohedral complexes of C_{82} fullerenols with different numbers of O and OH functional groups, which were synthesized in a high-temperature experiment and characterized by mass spectrometry. The reactivity of $Gd@C_{82}O_x(OH)_y$ endohedral complexes was estimated using the calculations of chemical electrophilicity (ω) and absolute electronegativity (χ) indices. It was found that the gadolinium guest atom increases the reactivity of fullereneol endohedral complexes with different ROSs. The endohedral complexes are proposed to be used for various MRI biomedical applications.

2. Experimental Procedures

A mixture of the Gd_2O_3 powder and graphite in a weight ratio of 1:1 was processed in high-frequency arc plasma discharge by sputtering of graphite electrodes with 3-mm axial holes [32] with very low chemical yield. Fullerene mixture was extracted from carbon condensate by carbon disulfide in a Soxhlet apparatus. Using the technique described by Akiyama et al., a mixture of $Gd@C_{82}$ and higher fullerenes was isolated from the resulting solution. The sample was dried and redissolved in toluene. The $Gd@C_{82}$ fullerene was isolated from the solution by high-efficiency liquid chromatography on Agilent Technologies 1200 Series chromatograph with the only one $Gd@C_{82}$ endohedral complex detected in the mass spectrum, which signal clearly stands out against broadband background noise (Figure S1).

According to the method proposed by Chiang and co-workers [12], the -O and -OH groups were attached to the isolated endohedral metallofullerene. Taking into account that the number of OH groups attached to the fullerene must be even [13,14], the composition of this product can be assumed as $Gd@C_{82}O_x(OH)_y$ ($x = 10-12$, $y = 30-32$, $x + y = 40-42$) [27].

3. Computational Details

The atomic and electronic structures of C_{82} fullerene, $Gd@C_{82}$ endohedral complex, and $Gd@C_{82}O_x(OH)_y$ fullerenols and energy of solvation (Figure 1) were calculated using DFT meta-hybrid exchange correlation MN15 functional [33] and def(2)-SVP basis set [34] for carbon (C), oxygen (O), and hydrogen (H) atoms and def(2)-SVP_ECP basis set for the gadolinium atom [35] using Gaussian 09 code [36]. The MN15 functional has a broader accuracy than any DFT potentials to reproduce bond energies, atomization energies, ionization potentials, electron affinities, proton affinities, reaction barrier heights, non-covalent interactions, hydrocarbon thermochemistry, isomerization energies, electronic excitation energies, absolute atomic energies, and molecular structures. In particular, it provides very accurate results for multi-, single-configurational, and non-covalent systems with mean unsigned error (MUE) 4.75, 1.85, and 0.25 kcal/mol, respectively, which is several times smaller than MUEs of conventional DFT potentials. The def(2)-SVP basis set is a balanced basis set to provide split valence, triple zeta valence, and quadruple zeta valence quality for H to Rn, which allows one to properly describe atomization energies, dipole moments, and structure parameters using density functional theory. The electronic structure calculations were performed within the restricted open-shell and unrestricted electronic structure calculations taking into account solvation effects using Universal solvation model based on density (SMD) [37]. Some details of taking into account solvation effects are presented in the SI Section.

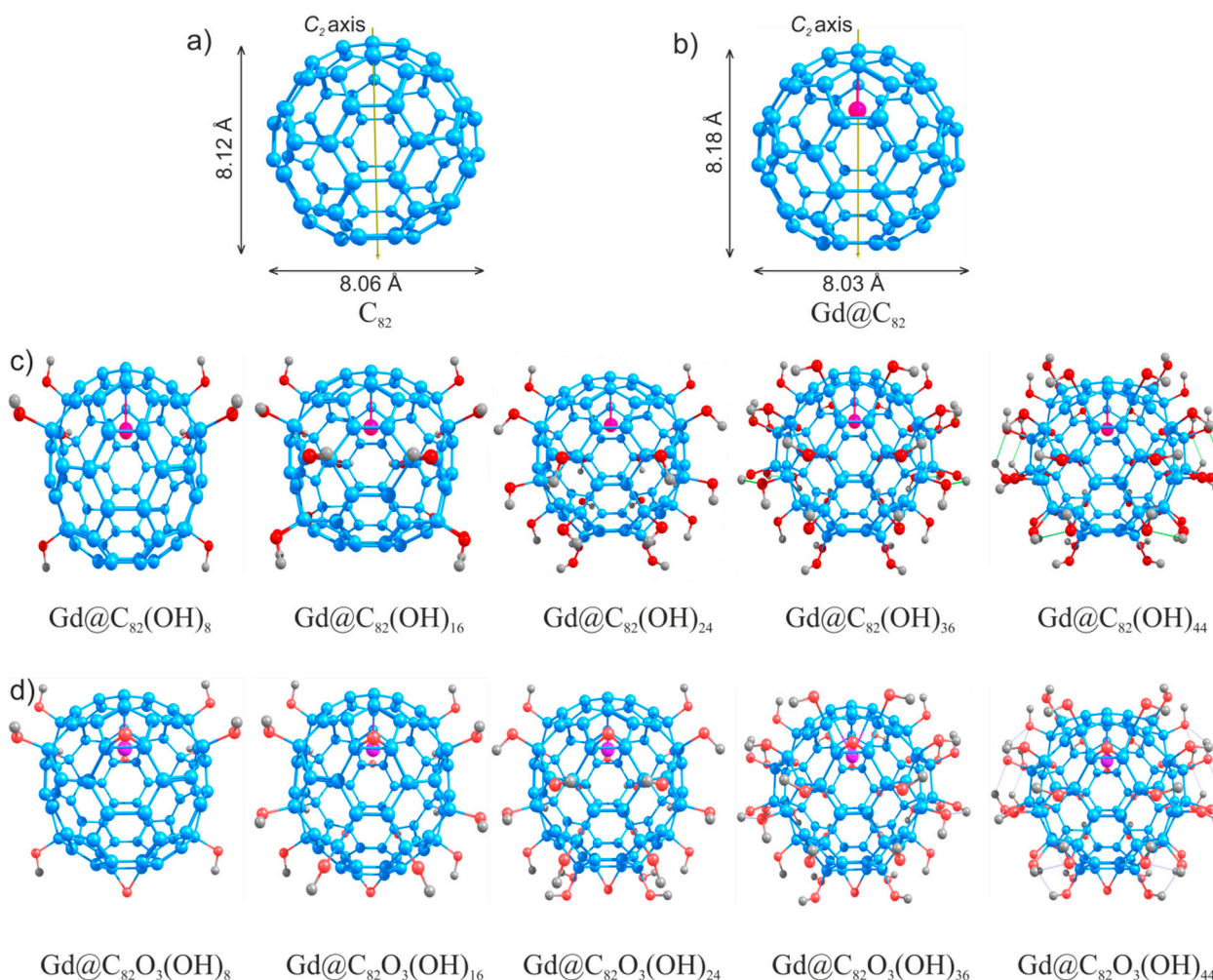


Figure 1. C₈₂ fullerene related clusters oriented following C_{2v} symmetry. (a) C₈₂, (b) Gd@C₈₂, (c) C₈₂O_x(OH)_y, and (d) Gd@C₈₂O_x(OH)_y ($x = 0, 3; y = 8, 16, 24, 36, 44$). Carbon, gadolinium, oxygen, and hydrogen atoms are shown in blue, fuchsia, red, and gray colors, respectively. The carbon cage lengths along the second-order axis for C₈₂ and Gd@C₈₂ are 8.12 and 8.18 Å with the widths 8.06 and 8.03 Å, respectively.

The Gd@C₈₂ optimization was performed with spin $S = 7/2$, which corresponds to $4f^7$ configuration of Gd⁺³ ion [38] (Figure 1a,b). The symmetrically distributed OH groups over the Gd@C₈₂ were employed to develop the atomistic models of different fullerlenols and to calculate their atomic and electronic structures (Figure 1c). The fullerlenols with three epoxy groups Gd@C₈₂O₃(OH)_y ($y = 8, 16, 24, 36, 44$) (Figure 1d) were developed by the uniform arrangement of hydroxyl and epoxy groups over fullerene carbon cage to reduce the number of possible intramolecular interactions and the atomic and electronic structures were studied as well. Some details of the development of structural models of Gd endohedral complexes of fullerlenols are presented in the SI Section.

To estimate the chemical reactivity of fullerlenol gadolinium endohedral complexes, the absolute electronegativity index $\chi = (I - A)/2$ (eV) [39], where I is the energy of the highest occupied molecular orbital (HOMO) and A is the energy of the lowest unoccupied molecular orbital (LUMO), and electrophilicity indexes $\omega = \chi^2/2\eta$ ($\eta = -(I - A)/2$ (in electron Volts, eV), which characterize the tendency of a molecule to attack the nucleophile, were calculated using the results of electronic structure calculations. The antioxidant properties of the fullerlenols were estimated by calculating the electronic characteristics of oxygen molecules with different multiplicities (m) and charges (z), namely for O₂⁻ $m = 2$ and $z = -1$; for O₂⁰ $m = 1$ and $z = 0$; for O₂⁰ $m = 3$ and $z = 0$; for hydrogen peroxide

molecules H_2O_2 $m = 1$ and $z = 0$; and for HOO^\bullet $m = 2$ and $z = 0$. The density of states for fullerene and its derivatives were calculated with a peak smearing of 0.3 eV.

4. Results and Discussion

4.1. The $\text{C}_{82}\text{O}_x(\text{OH})_y$ and $\text{Gd@C}_{82}\text{O}_x(\text{OH})_y$ Atomic Structures

The Gd guest atom in the Gd@C_{82} endohedral complex is coordinated to the center of the hexagon on the C_{2v} axis of the C_{82} cage [38]. An isolated Gd atom has the electron configuration $4f^7 5d^1 6s^2$ and Gd^{3+} ion has a $4f^7$ configuration, which points out that Gd 5d- and Gd 6s-electrons are transferred to the carbon sphere, forming ionic bonds between Gd ion and C_{82} cage. The Gd $4f^7$ configuration is consistent with the $\text{Gd}^{3+}\text{@C}_{82}^{3-}$ ion model [40]. The Gd@C_{82} ground spin state results from the intramolecular antiferromagnetic exchange between gadolinium ion with spin $S_{\text{Gd}} = 7/2$ and $S_{\text{C}_{82}} = 1/2$ [38] with the total spin $S_{\text{Gd@C}_{82}} = 6/2$ of the complex.

The C_{82} fullerene of C_{2v} symmetry consists of 12 pentagons and 32 hexagons (Figure 1a, Table 1). The formation of Gd@C_{82} leads to the elongation of some carbon–carbon bonds from 1.42–1.43 to 1.44–1.45 Å ($\Delta l = 0.02$ Å) (Table 1). In fullerenols, the C–C bond lengths are almost independent upon the number and positioning of the hydroxyl groups (8, 16, and 24) on the fullerene cage ($l = 1.38$ – 1.42 Å), as compared with pristine fullerene (Figure 2a, Table 1). However, an increase in the number of hydroxyl groups to 36 and 44 significantly changes the bond length, thus the global C_{82} π system is almost annihilated with conversion of aromatic C–C bonds to separate single and double bonds with increases of the length of the single bond from 1.41–1.42 to 1.51–1.53 Å ($\Delta l = 0.10$ – 0.12 Å), while the length of the double bond decreases from 1.38–1.41 to 1.33–1.35 Å ($\Delta l = 0.06$ – 0.08 Å). In addition to the bond length, the angles between the carbon atoms of the carbon hexagon to which the gadolinium ion is coordinated also change, decreasing by 1–3 degrees in comparison with $\text{C}_{82}\text{O}_x(\text{OH})_y$.

Table 1. Structural parameters * of $\text{Gd@C}_{82}\text{O}_x(\text{OH})_y$ and $\text{C}_{82}\text{O}_x(\text{OH})_y$ complexes.

Bond Lengths and Bond Angles	Complexes				
	$\text{C}_{82}(\text{OH})_y$				
	$\text{C}_{82}(\text{OH})_8$	$\text{C}_{82}(\text{OH})_{16}$	$\text{C}_{82}(\text{OH})_{24}$	$\text{C}_{82}(\text{OH})_{36}$	$\text{C}_{82}(\text{OH})_{44}$
$l(\text{C}_1\text{--}\text{C}_2)$	1.42	1.41	1.42	1.53	1.53
$l(\text{C}_2=\text{C}_3)$	1.41	1.41	1.41	1.35	1.33
$\angle\text{C}_{1-2-3}$	121	121	121	124	123
$\angle\text{C}_{1-2-4}$	109	109	109	109	112
$\angle\text{C}_{3-2-4}$	122	122	121	118	122
$\text{Gd@C}_{82}(\text{OH})_y$					
	$\text{Gd@C}_{82}(\text{OH})_8$	$\text{Gd@C}_{82}(\text{OH})_{16}$	$\text{Gd@C}_{82}(\text{OH})_{24}$	$\text{Gd@C}_{82}(\text{OH})_{36}$	$\text{Gd@C}_{82}(\text{OH})_{44}$
$l(\text{C}_1\text{--}\text{C}_2)$	1.42	1.41	1.41	1.52	1.51
$l(\text{C}_2=\text{C}_3)$	1.41	1.41	1.40	1.35	1.33
$\angle\text{C}_{1-2-3}$	119	120	120	121	122
$\angle\text{C}_{1-2-4}$	108	109	109	109	113
$\angle\text{C}_{3-2-4}$	125	121	121	119	122
$\text{C}_{82}\text{O}_x(\text{OH})_y$					
	$\text{C}_{82}\text{O}_3(\text{OH})_8$	$\text{C}_{82}\text{O}_3(\text{OH})_{16}$	$\text{C}_{82}\text{O}_3(\text{OH})_{24}$	$\text{C}_{82}\text{O}_3(\text{OH})_{36}$	$\text{C}_{82}\text{O}_3(\text{OH})_{44}$
$l(\text{C}_1\text{--}\text{C}_2)$	1.42	1.41	1.41	1.53	1.53
$l(\text{C}_2=\text{C}_3)$	1.41	1.41	1.41	1.35	1.33
$\angle\text{C}_{1-2-3}$	121	121	120	124	123
$\angle\text{C}_{1-2-4}$	109	109	109	109	113
$\angle\text{C}_{3-2-4}$	122	122	122	119	122

Table 1. Cont.

	Gd@C ₈₂ O _x (OH) _y				
	Gd@C ₈₂ O ₃ (OH) ₈	Gd@C ₈₂ O ₃ (OH) ₁₆	Gd@C ₈₂ O ₃ (OH) ₂₄	Gd@C ₈₂ O ₃ (OH) ₃₆	Gd@C ₈₂ O ₃ (OH) ₄₄
$l(C_1-C_2)$	1.42	1.42	1.41	1.53	1.52
$l(C_2=C_3)$	1.41	1.41	1.38	1.33	1.33
$\angle C_{1-2-3}$	120	120	120	123	122
$\angle C_{1-2-4}$	109	109	109	109	112
$\angle C_{3-2-4}$	123	123	122	118	121

C₈₂: $l(C_1-C_2) = 1.43$, $l(C_2=C_3) = 1.42$, $\angle C_{1-2-3} = 121$, $\angle C_{1-2-4} = 108$, $\angle C_{3-2-4} = 121$;
Gd@C₈₂: $l(C_1-C_2) = 1.45$, $l(C_2=C_3) = 1.44$, $\angle C_{1-2-3} = 121$, $\angle C_{1-2-4} = 107$, $\angle C_{3-2-4} = 121$

* Bond lengths (Å), bond angles (°).

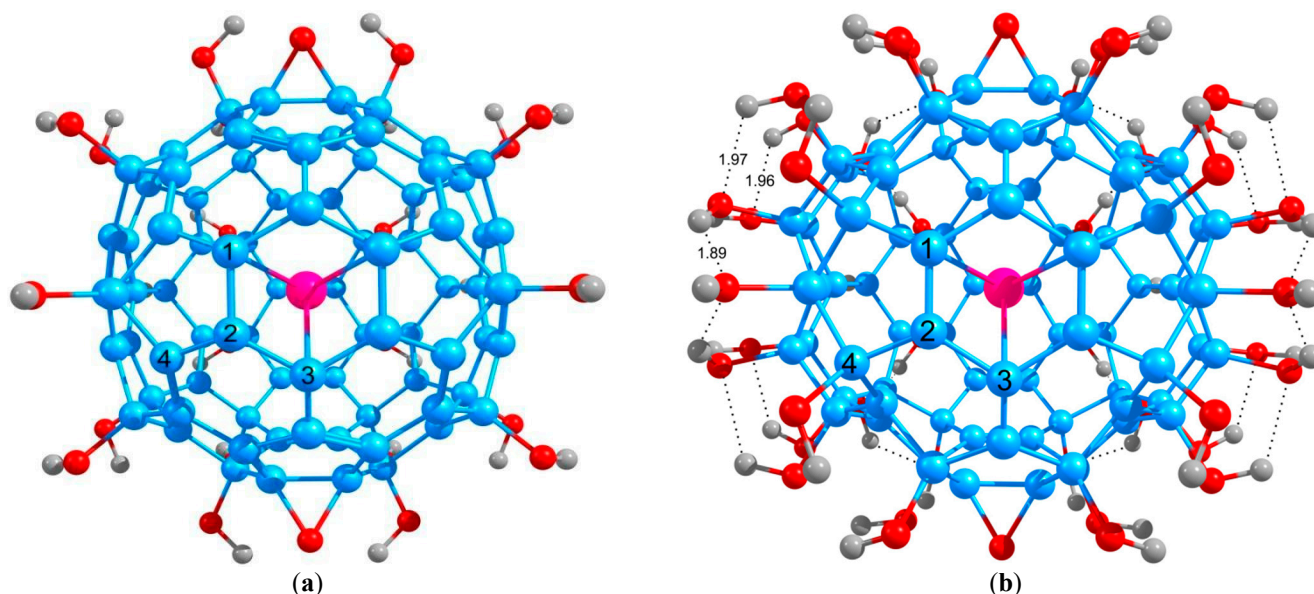


Figure 2. Atomic structure of Gd endohedral complexes of C₈₂ fullerenols. (a) Gd@C₈₂O₃(OH)₂₄ and (b) Gd@C₈₂O₃(OH)₄₄. Carbon, gadolinium, oxygen, and hydrogen atoms are presented in blue, fuchsia, red, and gray colors, respectively. Carbon atoms 1 and 2 are bonded through single bond, and carbon atoms 2 and 3 are bonded through double bond. (a) The bond lengths $l(C_1-C_2)$ and $l(C_2=C_3)$ in Gd@C₈₂O₃(OH)₂₄ are 1.41 and 1.38 Å, respectively. The bond angles $\angle C_{1-2-3}$, $\angle C_{1-2-4}$, and $\angle C_{3-2-4}$ are 120°, 109°, and 122°, respectively. (b) The bond lengths $l(C_1-C_2)$ and $l(C_2=C_3)$ in Gd@C₈₂O₃(OH)₄₄ are 1.52 and 1.33 Å, respectively. The bond angles $\angle C_{1-2-3}$, $\angle C_{1-2-4}$, and $\angle C_{3-2-4}$ are 122°, 112°, and 121°, respectively. The dotted lines show the hydrogen bonds between hydrogen and oxygen atoms of different hydroxyl groups with bond lengths from 1.89 to 1.97 Å.

The presence of gadolinium ion combined with epoxy and hydroxyl groups (8, 16 and 24) in the C₈₂ fullerene slightly changes the bond angles between carbon atoms (Figure 2a, Table 1). A greater number of hydroxyl groups increases the angle $\angle C_{1-2-3}$ by 2–4°, from 120° to 124°, $\angle C_{1-2-4}$ increases by 3–4°, from 109° to 112–113°, and $\angle C_{3-2-4}$ decreases by 3–4°, for $x = 36$ hydroxyl groups from 122–125° to 118–119°. For $x = 44$ hydroxyl groups, the angles increase by 3–4°, as compared with the fullerenols with 36 hydroxyl groups from 118–119° to 121–122°.

It can be seen (Figures 1 and 2, Table 1) that C₈₂O_x(OH)_y and Gd@C₈₂O_x(OH)_y ($x = 0, 3$; $y = 8, 16, 24, 36, 44$) complexes can be assigned to two different groups, namely: (1) $x = 0, 3$ and $y = 8, 16, 24$ and (2) $x = 0, 3$; $y = 36, 44$. In the first group, the π -system is maintained even in the presence of gadolinium ion in the carbon cage, which can be seen for the fullerenols from the change in the angle of the hexagon with the gadolinium ion coordinated to the center (a change by 0–2 degrees relative to that in C₈₂ and Gd@C₈₂ Figure 2a, Table 1). However, as the number of hydroxyl groups increases, global C₈₂

π -system is annihilated and uniform aromatic C-C bonds are replaced by the single and double bonds, which leads to a change in the geometry of the carbon cage (Figure 2b, Table 1).

The presence of 8, 16, and 24 hydroxyl groups on C_{82} carbon cage does not imply their significant mutual interaction (Figure 2a). When the number of hydroxyl groups increases to 36 and 44, they become close enough to each other and start interacting, forming a system of hydrogen bonds (Figure 2b). In particular, the distances between oxygen atoms of one hydroxyl group and hydrogen atoms of the other hydroxyl group ranges from 1.89 to 1.97 Å (Figure 2b).

The electronic structure calculations show that in $C_{82}O_x(OH)_y$ complexes with 8, 16, and 24 OH groups, the energy of interaction with solvent increases from 213 to 402 kJ/mol (Table S1), whereas $Gd@C_{82}O_x(OH)_y$ complex solvation is energetically favorable for 16 hydroxyl groups (793 kJ/mol, Table S1). An increase of the number of substituent hydroxyl groups in $C_{82}O_x(OH)_y$ and $Gd@C_{82}O_x(OH)_y$ ($x = 0, 3$; $y = 36, 44$) complexes leads to the formation of hydrogen bonds between oxygen and hydrogen atoms of the adjacent hydroxyl groups (the distance between hydroxyl groups decreased to 1.89–1.97 Å; Figure 2b). The energy of solvation was calculated for the complexes with larger numbers of $C_{82}O_8(OH)_y$ ($y = 8, 16, 24, 36, 44$) epoxy groups (Table S1). For the complexes with 8, 16, and 24 OH groups, the energy of interaction with the solvent increases from 165 to 298 kJ/mol (Table S1); for the complexes with 36 hydroxyl groups, it decreases to 258 kJ/mol; and for the complex with 44 hydroxyl groups, it increases to 288 kJ/mol (Table S1). The presence of gadolinium ion further increases the energy of solvation to 712–793 kJ/mol. All fullerenols have good solubility in water whether or not they have endohedral guest atom inside the C_{82} carbon cage. Consequently, for the complexes with a large number of hydroxyl groups, the interaction with the solvent is weaker (Table S1). The carbon cage is strongly distorted in the case of 36 and 44 hydroxyl groups, which leads to the breakdown of the π -system for the entire molecule and decreasing the electron affinity for the fullereneol, which is, according to the Koopmans theorem, the negative of LUMO energy, (Table 1, Figure 2b).

4.2. The $C_{82}O_x(OH)_y$ and $Gd@C_{82}O_x(OH)_y$ Electronic Structures

In Figure 3, the HOMO and LUMO diagrams are presented for free-standing Gd atom, C_{82} fullerene (C_{2v} symmetry) in gas phase, and $Gd@C_{82}$, and $Gd@C_{82}O_3(OH)_{24}$ complexes in solvent as well as O_2^0 ($m = 1, m = 3$), O_2^- ($m = 2$), and HOO^\bullet in the solvent.

The coordination type of epoxy groups of $C_{82}O_3(OH)_{24}$ fullereneols (Figures S2 and S3) slightly affects both HOMO and LUMO energies. In particular, the $\Delta E_{(HOMO-LUMO)}$ value for $C_{82}O_3(OH)_{24}$ is increased by 0.032 eV relative to that of $C_{82}(OH)_{24}$ (Figures S2 and S3), keeping spatial localization of the HOMO and LUMO orbitals almost intact. The 4f Gd electrons lie below HOMO by 1.88 eV in the energy region from -6.24 to -6.69 eV. The HOMO states are localized mainly on carbon atoms of the fullereneol (Figure 3b–d), and, so the total high spin moment of the complex is maintained. The HOMO and LUMO of the C_{82} fullerene are located at the top of the carbon cage (Figure 3b). In the Gd endohedral complex, the localization of α and β HOMOs is determined by endohedral gadolinium ion mostly at the top of the molecule in the vicinity of the carbon hexagon which coordinates Gd^{+3} (Figure 3c,d).

In this case, the spin-up and spin-down LUMOs are mostly localized at the carbon cage (Figure 3c). The hydroxy- and epoxy groups drive the localization of HOMOs and LUMOs states, i.e., the HOMO electron density is concentrated on carbon atoms near gadolinium and, vice versa, the LUMO electron density is localized at the opposite pole of the cage (Figure 3d).

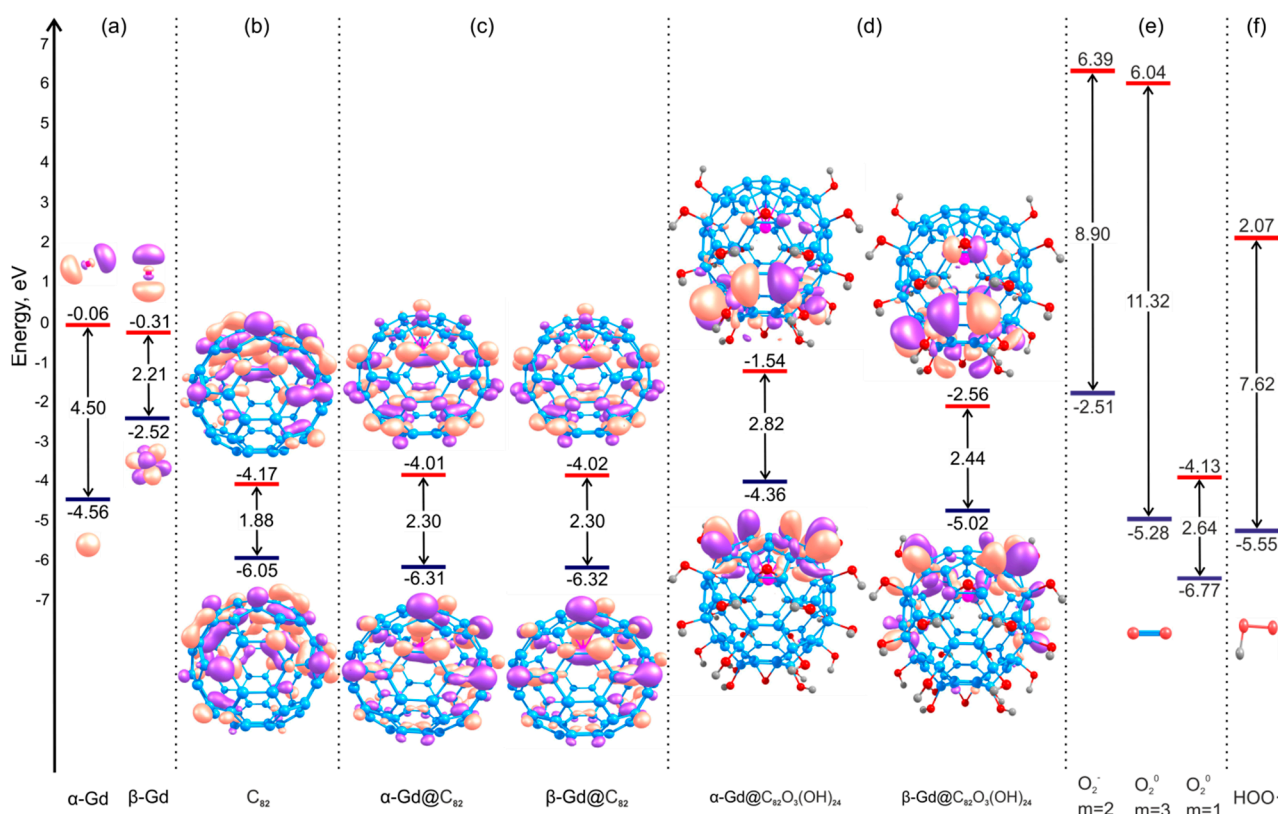


Figure 3. Diagram of the boundary molecular orbitals. (a) Gd, (b) C₈₂, (c) Gd@C₈₂, (d) Gd@C₈₂O₃(OH)₂₄, (e) O₂⁰ (*m* = 1, *m* = 3), O₂⁻ (*m* = 2), and (f) HOO• in the solvent. The HOMO and LUMO levels are shown in blue and red colors, respectively. The number between the HOMO and LUMO is the energy gap ($\Delta E_{\text{HOMO-LUMO}}$) in eV. The regions of the positive and negative wave functions on the molecules are shown in pink and purple colors.

Gadolinium ion slightly affects the energy shift of the occupied and unoccupied states. HOMO is shifted downwards by 0.26 eV from -6.05 to -6.31 (-6.32) eV, whereas the LUMO is shifted upward by 0.10 eV from -4.17 to -4.01 (-4.02) eV with an energy gap increasing by 0.42 eV from 1.88 to 2.30 eV relative to the value for the free-standing C₈₂ fullerene (Figure 3c). The coordination of epoxy and hydroxyl groups led to a shift of α -HOMO upward by 1.95 eV from -6.31 to -4.36 eV and shift of α -LUMO upward by 2.47 eV from -4.01 to -1.54 eV (Figure 3d). β -HOMO shifted upward by 1.3 eV from -6.32 to -5.02 eV and β -LUMO also shifted upward by 1.46 eV from -4.02 to -2.56 eV (Figure 3d). The energy gap for the β -electron of Gd@C₈₂O₃(OH)₂₄ is increased by 0.14 eV from 2.30 to 2.44 eV as compared with the pristine β -electron of Gd@C₈₂.

Let us analyze the HOMO-LUMO behavior to elucidate the charge transfer mechanisms between fullereneols and ROSes. The electronic structure of O₂ and HOO⁻ in different oxidation and spin states (O₂⁻ *m* = 2; O₂⁰ *m* = 1; O₂⁰ *m* = 3, Figure 3e,f) was previously studied by Dai et al. [41]. The O₂⁻ and O₂ HOMO energies (O₂⁻, *m* = 2; O₂⁰, *m* = 3) are in the energy region of $-2.51 \div -5.28$ eV with the energy region for LUMOs between 6.39 to 6.04 eV. Relative to the electronic structure of C₈₂O_x(OH)_y and Gd@C₈₂O_x(OH)_y (*x* = 0, 3; *y* = 8, 16, 24, 36, 44) fullereneols, the HOMO-LUMO energy gaps for O₂ species are much greater than the UV threshold (3.5 eV) and they are equal to 8.90 and 11.32 eV, respectively (Figure 3e). One can speculate that an electronic excitation that is less demanding in energy is an excitation from a reactive oxygen species to fullereneol LUMO states with alpha and beta energies equal to -1.54 and -2.56 eV, respectively. For a neutral singlet oxygen molecule, the HOMO-LUMO gap is 2.64 eV; therefore, the excited electrons may be transferred to the fullereneol's LUMO state (Figure 3e). The energies of HOMO and LUMO states of the hydroxyperoxide radical HOO• are -5.55 eV and 2.07 eV, respectively, with the HOMO-LUMO gap equal to 7.62 eV (Figure 3f), which is also greater than the UV

energy threshold. The α - and β -LUMO energies of fullereneol $\text{Gd@C}_{82}\text{O}_3(\text{OH})_{24}$ (-1.54 and -2.56 eV for α and β partners, Figure 3d) are also much lower than HOO^\bullet LUMO. The ROS molecules have large energy gaps and their unoccupied molecular orbitals are high in energy, which complicates the excitations of the electron from HOMOs to LUMOs. The boundary molecular orbitals of fullereneols are located between HOMOs and LUMOs of the ROSes; therefore, these molecules can easily interact with the chemical environment.

The electrophilicity ω and absolute electronegativity χ indices of $\text{Gd@C}_{82}\text{O}_x(\text{OH})_y$ and $\text{C}_{82}\text{O}_x(\text{OH})_y$ complexes are presented in Table 2. $\text{C}_{82}\text{O}_x(\text{OH})_y$ ($x = 0, 3; y = 16, 24$) exhibit no changes in the reactivity and their absolute electronegativity χ ranges from -4.5 to -4.9 eV. The guest gadolinium ion causes a change in reactivity in both α and β channels. In particular, the change in the properties of $\text{Gd@C}_{82}(\text{OH})_y$ ($y = 16, 24$) can be observed with absolute electronegativities χ from -3.8 and -3.1 eV for α electrons and from -5.1 to -3.5 eV—for β electrons. Variations of the coordinates of epoxy groups do not lead to strong differences in reactivity between α and β electrons. In particular, for 16 hydroxyl groups, the absolute electronegativities of α and β electrons are -3.2 eV, and for 24 hydroxyl groups, they are -2.9 and -3.8 eV, respectively.

Table 2. Electrophilicity and absolute electronegativity indices of $\text{Gd@C}_{82}\text{O}_x(\text{OH})_y$ and $\text{C}_{82}\text{O}_x(\text{OH})_y$ complexes.

Indexes	Complexes					
	$\text{C}_{82}\text{O}_3(\text{OH})_8$		$\text{C}_{82}\text{O}_3(\text{OH})_{16}$		$\text{C}_{82}\text{O}_3(\text{OH})_{24}$	
ω^*	7.3		5.2		11.6	
χ^{**}	-4.8		-4.5		-4.8	
	$\text{Gd@C}_{82}\text{O}_x(\text{OH})_y$					
	$\text{Gd@C}_{82}\text{O}_3(\text{OH})_8$		$\text{Gd@C}_{82}\text{O}_3(\text{OH})_{16}$		$\text{Gd@C}_{82}\text{O}_3(\text{OH})_{24}$	
	α	β	α	β	α	β
ω	13.0	6.5	5.7	5.8	3.1	5.8
χ	-4.3	-4.6	-3.2	-3.2	-2.9	-3.8

* ω —electrophilicity in eV, ** χ —absolute electronegativity in eV. C_{82} : $\chi = -5.1$ eV, $\omega = 13.9$ eV. Gd@C_{82} : (α) $\chi = -5.6$ eV, $\omega = 11.6$ eV; (β) $\chi = -5.2$ eV, $\omega = 11.7$ eV.

The $\text{C}_{82}\text{O}_3(\text{OH})_{24}$ complex has an electrophilicity index of $\omega = 11.6$ eV, which promotes chemical attacks of ROS nucleophiles. The guest gadolinium ion changes the ability to accept electrons in both α and β channels with $\omega = 5.76$ eV for 16 hydroxyl groups and 3.1 and 5.86 eV for 24 hydroxyl groups for α and β electrons, respectively.

5. Conclusions

The $\text{C}_{82}\text{O}_x(\text{OH})_y$ and $\text{Gd@C}_{82}\text{O}_x(\text{OH})_y$ ($x = 0, 3; y = 8, 16, 24, 36, 44$) complexes perspective for biomedical applications were synthesized and characterized using mass-spectroscopy. Following mass-spectrometry experimental detection, a number of atomistic models of endohedral fullereneols $\text{Gd@C}_{82}\text{O}_x(\text{OH})_y$ ($x = 0, 3; y = 8, 16, 24, 36, 44$) were developed and studied using ab initio DFT calculations. It was shown that the guest Gd atom promotes the chemical reactivity and electrophilic properties of fullereneol cages. For a relatively small number of hydroxyl groups, the C_{82} carbon cage of $\text{C}_{82}\text{O}_x(\text{OH})_y$ and $\text{Gd@C}_{82}\text{O}_x(\text{OH})_y$ ($x = 0, 3; y = 24$) complexes still maintain the π -electron system. The complexes display high electron affinity, which ensures advanced antioxidant properties. Increasing the number of hydroxyl groups ($y > 24$) in $\text{Gd@C}_{82}\text{O}_x(\text{OH})_y$ complexes leads to the formation of intramolecular hydrogen bonds between the hydroxyl groups, which prevents chemical interactions with water solvent with decreasing of reactivity and solubility of the complexes with consequent degradation of antioxidant properties. Based on combined experimental and theoretical investigation, the endohedral $\text{Gd@C}_{82}\text{O}_x(\text{OH})_y$ complexes with 24 hydroxyl groups are considered as the best candidate for biomedical applications.

Supplementary Materials: The following are available online at <https://www.mdpi.com/article/10.3390/computation9050058/s1>, Figure S1: Mass spectrum of the chromatographic fraction with Gd@C82 (positive mode); Description of Solvation models; Table S1: Energy of solvation of Gd@C₈₂O₃(OH)_y, C₈₂O₃(OH)_y and C₈₂O₈(OH)_y; Figure S2: Diagram of the boundary molecular orbitals of C₈₂O_x(OH)₂₄, Gd@C₈₂O_x(OH)₂₄ (x = 0, 3), O₂₀ (χ = 1, χ = 3), O²⁻ (χ = 2), and HOO• in the solvent (H₂O). The HOMO and LUMO levels are shown in blue and red color, respectively. The number between the HOMO and LUMO is the energy gap (ΔE_{HOMO-LUMO}, eV); Figure S3. Densities of states of Gd@C₈₂O_x(OH)_y. TDOS is total density of states, PDOS is partial density of states. Gd, C₈₂ and Gd@C₈₂ were calculated in gas phase, Gd@C₈₂O₃(OH)₂₄ in water solvent. (a) Gd: TDOS is shown in red color and multiplied by 0.5, PDOS of α-β-channels are shown in blue and green colors, respectively; (b) C₈₂: TDOS is shown in blue color; (c) Gd@C₈₂: TDOS is shown in red color and multiplied by 0.5, PDOS of α-β-channels are shown in blue and green colors; (d) Gd@C₈₂O₃(OH)₂₄: TDOS is shown in red color and multiplied by 0.5, PDOS of α-β-channels are shown in blue and green colors. Dotted line shows HOMO-LUMO energy gap ΔE; Cartesian coordinates of all calculated complexes.

Author Contributions: Conceptualization, O.N.T., S.G.O. and P.V.A.; Synthesis of fullerenols, N.G.V. and G.N.C.; Experimental study of biological activity, N.S.K.; Mass-spectroscopy characterization, A.A.S.; Quantum chemical calculations, F.N.T. and V.A.P. All authors have read and agreed to the published version of the manuscript.

Funding: The experimental results were funded by RFBR project No. 18-29-19003 MK. The quantum chemical study was funded by project 0721-2020-0033 of the Russian Ministry of Science and Education. The collaboration and coordination of Russian and Korean teams was supported by Collaborative NRF-RFBR grant (Korean ID: NRF-2019K2A9A1A06100125; Russian ID: Project No. 19-53-51005 NIFa RFFI-Korea) and NRF 2021R1A2C1010455 grant.

Institutional Review Board Statement: Not Applicable.

Informed Consent Statement: Not Applicable.

Data Availability Statement: All supporting data can be found in SI section available online.

Acknowledgments: The experimental results were funded by RFBR project No. 18-29-19003 MK. The quantum chemical study was funded by project 0721-2020-0033 of the Russian Ministry of Science and Education. The collaboration and coordination of Russian and Korean teams was supported by Collaborative NRF-RFBR grant (Korean ID: NRF-2019K2A9A1A06100125; Russian ID: Project No. 19-53-51005 NIFa RFFI-Korea) and NRF 2021R1A2C1010455 grant.

Conflicts of Interest: The authors declare no conflict of interest.

References

1. Popov, A.A.; Yang, S.; Dunsch, L. Endohedral Fullerenes. *Chem. Rev.* **2013**, *113*, 5989–6113. [[CrossRef](#)]
2. Shinohara, H. Endohedral metallofullerenes. *Rep. Prog. Phys.* **2000**, *63*, 843–892. [[CrossRef](#)]
3. Yang, S.; Wei, T.; Jin, F. When metal clusters meet carbon cages: Endohedral clusterfullerenes. *Chem. Soc. Rev.* **2017**, *46*, 5005–5058. [[CrossRef](#)] [[PubMed](#)]
4. Wang, Z.; Gao, X.; Zhao, Y. Mechanisms of Antioxidant Activities of Fullerenols from First-Principles Calculation. *J. Phys. Chem.* **2018**, *122*, 8183–8190. [[CrossRef](#)]
5. Zhang, J.; Ye, Y.; Chen, Y.; Pregot, C.; Li, T.; Balasubramanian, S.; Hobart, D.B.; Zhang, Y.; Wi, S.; Davis, R.M.; et al. Gd₃N@C₈₄(OH)_x: A New Egg-Shaped Metallofullerene Magnetic Resonance Imaging Contrast Agent. *J. Am. Chem. Soc.* **2014**, *136*, 2630–2636. [[CrossRef](#)]
6. Da Ross, T. Twenty Years of Promises: Fullerene in Medicinal Chemistry. In *Medicinal Chemistry and Pharmacological Potential of Fullerenes and Carbon Nanotubes*; Cataldo, F., Da Ros, T., Eds.; Carbon Materials: Chemistry and Physics; Springer: Dordrecht, The Netherlands, 2008; Volume 1. [[CrossRef](#)]
7. Kang, S.G.; Huynh, T.; Zhou, R. Non-destructive Inhibition of Metallofullerenol Gd@C₈₂(OH)₂₂ on WW domain: Implication on Signal Transduction Pathway. *Sci. Rep.* **2012**, *2*, 957. [[CrossRef](#)]
8. Kang, S.G.; Zhou, G.; Yang, P.; Liu, Y.; Sun, B.; Huynh, T.; Meng, H.; Zhao, L.; Xing, G.; Chen, C.; et al. Molecular mechanism of pancreatic tumor metastasis inhibition by Gd@C₈₂(OH)₂₂ and its implication for de novo design of nanomedicine. *Proc. Natl. Acad. Sci. USA* **2012**, *109*, 15431–15436. [[CrossRef](#)] [[PubMed](#)]
9. Meng, J.; Liang, X.; Chen, X.; Zhao, Y. Biological characterizations of [Gd@C₈₂(OH)₂₂]_n nanoparticles as fullerene derivatives for cancer therapy. *Integr. Biol.* **2013**, *5*, 43–47. [[CrossRef](#)]

10. Churilov, G.N.; Kratschmer, W.; Osipova, I.V.; Glushenko, G.A.; Vnukova, N.G.; Kolonenko, A.L.; Dudnik, A.I. Synthesis of fullerenes in a high-frequency arc plasma under elevated helium pressure. *Carbon* **2013**, *62*, 389–392. [[CrossRef](#)]
11. Akiyama, K.; Hamano, T.; Nakanishi, Y.; Takeuchi, E.; Noda, S.; Wang, Z.; Kubuki, S.; Shinohara, H. Non-HPLC rapid separation of metallofullerenes and empty cages with TiCl_4 Lewis acid. *J. Am. Chem. Soc.* **2012**, *134*, 9762–9767. [[CrossRef](#)] [[PubMed](#)]
12. Chiang, L.Y.; Swirczewski, J.W.; Hsu, C.S.; Chowdhury, S.K.; Cameron, S.; Creegan, K. Multi-hydroxy additions onto C_{60} fullerene molecules. *J. Chem. Soc. Chem. Commun.* **1992**, *114*, 1791–1793. [[CrossRef](#)]
13. Shilin, V.A.; Szhogina, A.A.; Suyasova, M.V.; Sedov, V.P.; Lebedev, V.T.; Kozlov, V.S. Fullerenes and fullerlenols survival under irradiation. *Nanosystems* **2016**, *7*, 146–152. [[CrossRef](#)]
14. Wang, B.C.; Wang, H.W.; Tso, H.C.; Chen, T.L.; Chou, Y.M. Theoretical studies of $\text{C}_{70}(\text{OH})_n$ ($n = 14, 16, 18$ and 20) fullerols. *J. Mol. Struct. THEOCHEM* **2002**, *581*, 177–186. [[CrossRef](#)]
15. Aschberger, K.; Johnston, H.J.; Stone, V.; Aitken, R.J.; Tran, C.L.; Hankin, S.M.; Peters, S.A.K.; Christensen, F.M. Review of fullerene toxicity and exposure—Appraisal of a human health risk assessment, based on open literature. *Regul. Toxicol. Pharmacol.* **2010**, *58*, 455–473. [[CrossRef](#)] [[PubMed](#)]
16. Trpkovic, A.; Todorovic-Markovic, B.; Trajkovic, V. Toxicity of pristine versus functionalized fullerenes: Mechanisms of cell damage and the role of oxidative stress. *Arch. Toxicol.* **2012**, *86*, 1809–1827. [[CrossRef](#)] [[PubMed](#)]
17. Chen, C.; Xing, G.; Wang, J.; Zhao, Y.; Li, B.; Tang, J.; Jia, G.; Wang, T.; Sun, J.; Xing, L. Multihydroxylated $[\text{Gd}@\text{C}_{82}(\text{OH})_{22}]_n$ Nanoparticles: Antineoplastic Activity of High Efficiency and Low Toxicity. *Nano Lett.* **2005**, *5*, 2050–2057. [[CrossRef](#)] [[PubMed](#)]
18. Chen, Z.; Ma, L.; Liu, Y.; Chen, C. Applications of Functionalized Fullerenes in Tumor Theranostics. *Theranostics* **2012**, *2*, 238–250. [[CrossRef](#)]
19. Keshri, S.; Tembe, B.L. Thermodynamics of hydration of fullerols $[\text{C}_{60}(\text{OH})_n]$ and hydrogen bond dynamics in their hydration shells. *J. Chem. Phys.* **2017**, *146*, 074501. [[CrossRef](#)]
20. Djordjevic, A.; Srdjenovic, B.; Seke, M.; Petrovic, D.; Injac, R.; Mrdjanovic, J.J. Review of synthesis and antioxidant potential of fullereneol nanoparticles. *J. Nanomater.* **2015**, *2015*, 567073. [[CrossRef](#)]
21. Eropkin, M.Y.; Melenevskaya, E.Y.; Nasonova, K.V.; Bryazhnikova, T.S.; Eropkina, E.M.; Danilenko, D.M.; Kiselev, O.I. Synthesis and biological activity of fullerlenols with various contents of hydroxyl groups. *Pharm. Chem. J.* **2013**, *47*, 87–91. [[CrossRef](#)]
22. Kovel, E.S.; Sachkova, A.S.; Vnukova, N.G.; Churilov, G.N.; Knyazeva, E.M.; Kudryasheva, N.S. Antioxidant activity and toxicity of fullerlenols via bioluminescence signaling: Role of oxygen substituents. *Int. J. Mol. Sci.* **2019**, *20*, 2324. [[CrossRef](#)]
23. Kudryasheva, N.S.; Kovel, E.S.; Sachkova, A.S.; Vorobeva, A.A.; Isakova, V.G.; Churilov, G.N. Bioluminescent enzymatic assay as a tool for studying antioxidant activity and toxicity of bioactive compounds. *Photochem. Photobiol.* **2017**, *93*, 536–540. [[CrossRef](#)] [[PubMed](#)]
24. Sachkova, A.S.; Kovel, E.S.; Churilov, G.N.; Guseynov, O.A.; Bondar, A.A.; Dubinina, I.A.; Kudryasheva, N.S. On mechanism of antioxidant effect of fullerlenols. *Biochem. Biophys. Rep.* **2017**, *9*, 1–8. [[CrossRef](#)]
25. Sachkova, A.S.; Kovel, E.S.; Churilov, G.N.; Stom, D.I.; Kudryasheva, N.S. Biological activity of carbonic nano-structures—comparison via enzymatic bioassay. *J. Soils Sediments* **2019**, *19*, 2689–2696. [[CrossRef](#)]
26. Maravilla, K.R.; San-Juan, D.; Kim, S.J.; Elizondo-Riojas, G.; Fink, J.R.; Escobar, W.; Bag, A.; Roberts, D.R.; Hao, J.; Pitrou, C.; et al. Comparison of Gadoterate Meglumine and Gadobutrol in the MRI Diagnosis of Primary Brain Tumors: A Double-Blind Randomized Controlled Intraindividual Crossover Study (the REMIND study). *Am. J. Neuroradiol.* **2017**, *38*, 1681–1688. [[CrossRef](#)]
27. Ersoy, H.; Rybicki, F.J. Biochemical Safety Profiles of Gadolinium-Based Extracellular Contrast Agents and Nephrogenic Systemic Fibrosis. *J. Magn. Reson. Imaging.* **2007**, *26*, 1190–1197. [[CrossRef](#)]
28. Guan, M.; Ge, J.; Wu, J.; Zhang, G.; Chen, D.; Zhang, W.; Zhang, Y.; Zou, T.; Zhen, M.; Wang, C.; et al. Fullerene/photosensitizer nanovesicles as highly efficient and clearable phototheranostics with enhanced tumor accumulation for cancer therapy. *Biomaterials* **2016**, *103*, 75–85. [[CrossRef](#)]
29. Rodriguez-Galvan, A.; Rivera, M.; Garcia-Lopez, P. Gadolinium-containing carbon nanomaterials for magnetic resonance imaging: Trends and challenges. *J. Cell. Mol. Med.* **2020**, *24*, 3779–3794. [[CrossRef](#)]
30. Tang, J.; Zhang, R.; Guo, M. Gd-metallofullerene drug delivery system mediated macrophage polarization enhances the efficiency of chemotherapy. *J. Control. Release* **2020**, *320*, 293–303. [[CrossRef](#)] [[PubMed](#)]
31. Clavaguera, C.; Sansot, E.; Calvo, F.; Dognon, J.P. Gd(III) polyaminocarboxylate chelate: Realistic many-body molecular dynamics simulations for molecular imaging applications. *J. Phys. Chem.* **2006**, *110*, 12848–12851. [[CrossRef](#)]
32. Dudnik, A.I.; Vnukova, N.G.; Drokin, N.A.; Bondarev, V.S.; Shestakov, N.P.; Tomashevich, Y.V.; Churilov, G.N. Electrophysical properties of hydroxylated endohedral metallofullerene with gadolinium. *J. Phys. Chem. Solids.* **2019**, *135*, 109094. [[CrossRef](#)]
33. Yu, H.S.; He, X.; Li, S.L.; Truhlar, D.G. MN15: A Kohn–Sham global-hybrid exchange–correlation density functional with broad accuracy for multi-reference and single-reference systems and noncovalent interactions. *Chem. Sci.* **2016**, *7*, 5032–5051. [[CrossRef](#)]
34. Weigend, F.; Ahlrichs, R. Balanced basis sets of split valence, triple zeta valence and quadruple zeta valence quality for H to Rn: Design and assessment of accuracy. *Phys. Chem.* **2005**, *7*, 3297. [[CrossRef](#)] [[PubMed](#)]
35. Gulde, R.; Pollak, P.; Weigend, F. Error-Balanced Segmented Contracted Basis Sets of Double- ζ to Quadruple- ζ Valence Quality for the Lanthanides. *J. Chem. Theory Comput.* **2012**, *8*, 4062–4068. [[CrossRef](#)]
36. Frisch, M.J. *Gaussian 09, Revision A*, 1st ed.; Gaussian, Inc.: Wallingford, CT, USA, 2009.

37. Marenich, A.V.; Cramer, C.J.; Truhlar, D.G. Universal solvation model based on solute electron density and a continuum model of the solvent defined by the bulk dielectric constant and atomic surface tensions. *J. Phys. Chem.* **2009**, *113*, 6378–6396. [[CrossRef](#)] [[PubMed](#)]
38. Dolg, M.; Stoll, H.; Preuss, H. Energy-adjusted ab initio pseudopotentials for the rare earth elements. *J. Chem. Phys.* **1989**, *90*, 1730–1734. [[CrossRef](#)]
39. Pearson, R.G. *Chemical Hardness: Applications from Molecules to Solids*; Wiley: Weinheim, Germany, 1997.
40. Nishibori, E.; Iwata, K.; Sakata, M.; Takata, M.; Tanaka, H.; Kato, H.; Shinohara, H. Anomalous endohedral structure of Gd@C82 metallofullerenes. *Phys. Rev.* **2004**, *69*, 113412. [[CrossRef](#)]
41. Dai, X.; Gao, Y.; Xin, M.; Wang, Z.; Zhou, R. The ground state and electronic structure of Gd@C82: A systematic theoretical investigation of first principle density functional. *J. Chem. Phys.* **2014**, *141*, 244306. [[CrossRef](#)]